Solid-state synthesis and optical properties of ZnO and SnO_2 nanoparticles and their nanocomposites with SiO_2.

C. Diaz[a*], M. L.Valenzuela[b], M. Segovia, K. Correa[a], R. de la Campa[c] and A. Presa Soto[c*]

[a]*Departamento de Química, Facultad de Ciencias, Universidad de Chile, Las Palmeras 3425, Ñuñoa, Casilla 653, Santiago, Chile.*

[b]*Universidad Autónoma de Chile, Instituto de Ciencias Químicas Aplicadas, Inorganic Chemistry and Molecular Materials Center, el Llano Subercaseaux 2801, San Miguel, Santiago, Chile.*

[c] *Departamento de Química Orgánica e Inorgánica(IUQOEM). Facultad de Química. Universidad de Oviedo. Julián Clavería s/n, 33006, Oviedo (Spain).*

*E-mail: cdiaz@uchile.cl, and presaalejandro@uniovi.es

ABSTRACT

Nanostructured luminescent ZnO and SnO_2 materials are prepared by a solid-state method based on the pyrolysis of hybrid macromolecular precursors $ZnCl_2$●Chitosan and $SnCl_2$●Chitosan having different [polymer/MCl_2] (M = Zn or Sn) ratios (1:1, 1:5 and 1:10), under air at 800°C .The pyrolytic ZnO and SnO_2 nanomaterials show a dependence of the particle size, morphology and luminescent properties with the ratio [metal/polymer] in the MCl_2●Chitosan precursors. Thus, ZnO semiconductor materials exhibit luminescence spectra with several emission peaks between 300 and 600 nm. The most intense emission at 440 nm corresponds to a radiative transition of an electron from the shallow donor level of oxygen vacancies, and the zinc interstitial, to the valence band. All the ZnO materials synthesized show a rather intense green emission at ca. 573 nm, which is characteristic of this synthetic methodology. On the other hand, the photoluminescence spectrum of the nanostructured SnO_2 shows an intense blue luminescence at a wavelength of 420 nm which may be attributed to oxygen-related defects that have been introduced during the growth process of the nanoparticles. In other hand, whereas SnO_2 was successfully

incorporated into SiO_2 structure (SnO_2//SiO_2) by pyrolysis of solid-state mixtures of the precursors $SnCl_2$●Chitosan in the presence of SiO_2, the same reaction carried out with $ZnCl_2$●Chitosan precursors led to a mixture of Zn_2SiO_4 and SiO_2 The absorption and photoluminescence properties of the nanostructured SnO_2//SiO_2 were very similar than those of pure SnO_2. Thus, this new methodology yields nanostructured semiconductor materials, ZnO and SnO_2, suitable for optoelectronic and sensor solid-state devices.

Keywords: SnO_2, ZnO, solid-state synthesis, chitosan, SnO_2·SiO_2, ZnO·SiO_2

Introduction

Metal oxides materials are, in general, very useful semiconductors with a wide bandgap spanning the visible and UV, an interesting electronic properties,[1,2] and notable catalytic application.[3,4] Among the most important semiconductor metal oxides, SnO_2[5] and ZnO[6] have been extensively studied due to their interesting and practical applications.[7] Thus, SnO_2 is a wide band gap n-type semiconductor with significant importance in several technological applications such as gas sensing, Li-ion batteries, and solar cells.[8,9] For instance, it has been widely used as sensor in H_2 and CO detection.[7] Although several synthetic methods in solution have been reported for the preparation of SnO_2 materials,[8,9] only few solid-state methods leading to well characterized nanostructured SnO_2 materials have been described to date.[10] On the other hand, nanostructured ZnO is one of the most promising nanomaterials to be used in sensors due principally to its biocompatibility, chemical and photochemical stability, high specific surface area, optical transparency, electrochemical activity, and high electron mobility.[6] For instance, nanostructured ZnO materials have been successfully employed in the detection of biological

molecules.[11] As above (i.e. nanostructured SnO_2 materials), only few solid-state methods have been reported to date for the preparation of well-defined ZnO materials.[11,12]

Generally, the incorporation of metal-oxide nanoparticles into solid sensors is problematic when those have been produced *via* a solution phase method, because the solid-state isolation of the nanoparticles usually causes the nanoparticle agglomeration.[13] In this regard, the synthesis of nanoparticles directly from a solid-state approach might represent a more reliable method to achieve the incorporation of metal-oxides into sensors. Consequently the development of new solid-state methods to prepare metal-oxide nanoparticles is sought after. We have previously reported two solid-state methods allowing the synthesis of different metallic nanostructured materials (M, M_xO_y, and $M_xP_yO_z$) for a range of transition, valve and noble metals. The first methodology employed organometallic derivatives directly linked to poly- and cyclotriphosphazenes as molecular precursors of the metallic nanostructure,[14-17] while the second used solid-state mixtures of an appropriate organometallic moiety and cyclotriphosphazenes not possesing any coordinative functional group (i.e. cyclospirophosphazenes of general formula $[N=P(O_2C_{12}H_8)]_3$).[18] Both yielded the metal oxides together with pyrophosphate phases of the corresponding metal. For instance, when metals and metalloids were used both phases were observed, *i.e.* the metal oxide and the pyrophosphate. However, with noble metals, for which the formation of oxides or pyrophosphates is thermodynamically unfavored, the reduction with CO produced nanostructured M° materials during the molecular decomposition by pyrolysis.[18]

Among the different solid-state polymer templates that can be used for the synthesis of nanostructured metal oxides, Chitosan is one of the most promising macromolecules. Chitosan is derived from chitin, which is the second most abundant natural polymer after cellulose, and can be extracted mainly

from shrimp and krillby deacetylation with strong alkali bases.[19-21] The structure of Chitosan has been elucidated from molecular and crystal structure determination of both the hydrated and non-hydrated forms.[22] Chitosan is a biodegradable, biocompatible and non-toxic polysaccharide that, owing their interesting properties, it has received considerable attention in environmental, agricultural and biomedical applications.[23-25] One of the most interesting properties of Chitosan is related to its inherential high capacity to establish metal macromolecular complexes, and their high efficiency for metal uptaking from aqueous solutions.[26-28] To date, two metal complexation models are proposed; the bridge model (I)[29] in which chitosan metal complexes are created when both, amino (two or more) and hydroxyl side groups of the main chain are binded to the same metal centre (intra- or inter- molecular complexation may occur between the metal-ion and amine and hydroxyl groups from the same or different chains); and the pendant model (II), in which only one amine or hydroxyl group is acting as a pendant ligand. Studies based on ESR[30] and IR[31] suggested that the bridge model (I) is the most likely coordination pathway, whereas other studies based on X-ray[29] suggested the pendant model (II) as the most likely coordination mode. In consequence, the structure of macromolecular metal complexes of Chitosan is, so far, not well known.[30]

Here, we report a straightforward solid-state novel methodology to prepare stoichiometric and crystalline SnO_2 and ZnO metal-oxides nanoparticles. The method consists of the pyrolysis under air at 800°C of the macromolecular complexes $ZnCl_2$●Chitosan and $SnCl_2$●Chitosan, in which the chitosan is acting as solid state template, for the growth of the metal oxide nanoparticles. We studied the influence of the polymer/metal molar ratios over the final properties of the nanostructured metal-oxides (SnO_2 and ZnO), demonstrating that chitosan is acting as a valuable solid template that allows the formation of SnO_2 and ZnO nanoparticles with control of the particle size,

morphology, and luminescent properties. Also, here we present a method to incorporate SnO_2 and ZnO metal-oxides into SiO_2 structure by pyrolysis of the MCl_2●Chitosan (M= Zn and Sn) precursors in the presence of SiO_2 generated by a sol-gel method. The Uv-vis and photoluminescence properties of the synthesized metal-oxides were also studied.

Experimental

$ZnCl_2$▪$2H_2O$ and $SnCl_2$▪$6H_2O$ from Aldrich were used as received. Chitosan (Aldrich) of low molecular weight was also used as received. An estimation of the molecular weight was obtained by viscosity measurements and the Mark-Houwink equation. Thus, using parameters [h] previously reported by Brugnenotto, et al,[31] an aqueous solution of acetic acid, NaCl, and urea as a solvent, a value of M_W = 61000 was estimated. All the reactions were performed using CH_2Cl_2 as solvent.

Synthesis of the polymeric precursors $ZnCl_2$●Chitosan and $SnCl_2$●Chitosan

A typical procedure is described as follows: In a Schlenk flask, an appropriate amount of metallic chloride ($ZnCl_2$▪$2H_2O$ or $SnCl_2$▪$6H_2O$) and Chitosan were suspended in CH_2Cl_2 at different [Chitosan/MCl_2] molar ratios (1:1; 1:5, and 1:10). The heterogeneous mixture was stirred at room temperature for a given time (reaction time and additional details for each metal chloride reaction are given in Table S1 of Supplementary Materials). After removing the supernatant solution by decantation, the remained solid was dried under reduced pressure to give white materials. Due to their insolubility, the characterization of the

precursors was performed by ^{13}C-CP-MAS NMR spectroscopy, elemental analysis, FT-IR spectroscopy, and TG/DSC analysis. Approximate metal content was estimated from the elemental analysis and the TGA curves.

Incorporation of SnO_2 and ZnO into SiO_2

SiO_2 was prepared according with the literature procedures. Briefly, tetraethoxysilane (TEOS), ethanol, and acetic acid in a molar ratio of 1:4:4, were mixed with water (nanopure), and the mixture were stirring for 3 day. The obtained gel was dried at 100 °C under reduced pressure in a vacuum furnace. Mixtures of solid precursors [$ZnCl_2$●Chitosan] and [$SnCl_2$●Chitosan] were calcined at 800 °C for 2 h under air in the presence of as prepared SiO_2.

Pyrolysis of the precursors

Pyrolysis experiments were performed using 0.05–0.15 g of the metallic precursors, $ZnCl_2$●Chitosan and $SnCl_2$●Chitosan, in alumina boats. The samples were heated in a furnace (Daihan oven model Wise Therm FHP-12) under a flow of air from 25°C to upper temperature limits of 200°C, and then to 800 °C, followed by annealing at 800 °C for 2-4 h. The heating rate was fixed at 10 °C min^{-1} for all experiments.

Characterization of the pyrolytic products

The solid pyrolytic samples were characterized by X-Ray powders diffraction (XRD), scanning electron microscopy (SEM), high resolution transmission electron microscopy (HR-TEM), Fourier transform infra-red (FT-IR) spectroscopy, and thermogravimetric (TGA) and differential scanning

calorimetric (DSC) analysis. SEM images were acquired with a Philips EM 300 scanning electron microscope. Energy dispersive X-ray analysis (EDAX) was performed on a NORAN Instrument micro-probe attached to a JEOL 5410 scanning electron microscope. TEM data were acquired using a JEOL SX100 and a JEOL 2011 transmission electron microscope. HRTEM observations were performed using a JEOL 2000FX microscope at 200 kV. TEM samples were prepared by dispersing the pyrolyzed material onto copper grids and dried at room temperature. For high-resolution examination of graphitic carbons, flakes of sonicated carbons were dispersed on grids and examined under the SEM to determine their thickness. X-ray diffraction (XRD) was conducted at room temperature on a Siemens D-5000 diffractometer with θ-2θ geometry. XRD data was collected using Cu-*K*α radiation (40 kV, 30 mA). FTIR measurements were performed on a Perkin Elmer FT-IR spectrophotometer model Spectrum BXII.

Results and Discussion

1. Characterization of the polymeric precursors precursors, $ZnCl_2$●Chitosan and $SnCl_2$●Chitosan, prepared from different MCl_2/Chitosan ratios (1:1, 5:1 and 10:1, M = Zn or Sn).

The direct reaction of the metallic dichlorides, $SnCl_2$ and $ZnCl_2$, with Chitosan in CH_2Cl_2, yielded air stable polymeric precursor of general formula $ZnCl_2$●Chitosan and $SnCl_2$●Chitosan as a white solids. The reaction between the partially soluble Chitosan and the insoluble metallic chlorides, MCl_2 (M = Zn or Sn) ocurred in heterogeneous pahese. The equilibrium of the reaction was slowly moved toward the formation of very insoluble $ZnCl_2$●Chitosan and

$SnCl_2$●Chitosan precursors respectively. Due to the low solubility of the MCl_2 chlorides in CH_2Cl_2, the synthesis of the precursors were very slow, taking about 2 weeks to conclusion. The metal content in the precursors was determined by both elemental and TGA analysis. By both techniques the values were varying consistently from 89% to 94% of the initail ammount of MCl_2 used in each reaction (see Table S2 in Supplementary Materials). This result demonstrated that almost all the metal chloride used in the reaction is coordinated to chitosan. This is of pivotal importance in order to control the polymer/metal ratio in the final $ZnCl_2$●Chitosan and $SnCl_2$●Chitosan precursors. Both polymeric precursors were analyzed by ^{13}C-CP-MAS NMR spectroscopy showing the presence of Chitosan in the macromolecular complexes (see Supplementary Materials).[31-33] Moreover, the peaks were slightly shifted (downfield) with respect to those of free Chitosan evidencing the coordination of the metallic moiety to the polymeric backbone. The downfield shifting of the signals was more pronounced in the carbon directly linked to the coordinating NH_2 group (C_1 of the precursors was shifted (ca. 1ppm) from that of chitosan, see Supplementary Materials). However, this effect was not observed in the 1:10 $ZnCl_2$●Chitosan precursor because the metal content was very low (see Supplementary Materials). These deshelling in the ^{13}C-CP-MAS NMR signals was also observed in similar [Pt]●Chitosan complexes.[32]

TGA/DTA analyses also provided evidences of the coordination of Zn and Sn metal centers to the polymer backbone. For instance, the thermogram of the $ZnCl_2$●Chitosan precursor in 1:1 molar ratios exhibited very different weight loss pattern with respect to that of the free Chitosan (see Supplementary Materials).[34] Indeed, whereas the DTA curve of the free Chitosan showed a strong sharp exothermic peak at 290 °C, and two more exothermic peaks at 550 °C and 650 °C, the DTA curve of the Chitosan●$ZnCl_2$ (1:1) precursor showed

a peak at 250 °C, and only one broad peak at 550 °C due to the formation of ZnO, which evidenced the coordination of the Zn^{2+} centers to the chitosan. Also the final ceramic residue at 800 °C of the Chitosan●$ZnCl_2$ (1:1) precursor was higher (90 % of its initial mass) than that of chitosan as a result of the metal moiety coordination (non-coordinate MCl_2 species were eliminated during the CH_2Cl_2 filtration). Similar behavior was observed for the $ZnCl_2$●Chitosan having different metal loadings (1:5 and 1:10), as well as for the $SnCl_2$●Chitosan precursors (1:1, 1:5 and 1:10).

2. Characterization of the ZnO materials

2.1. Crystallographic and electronic microscopy characterization of ZnO materials. X-Ray powder diffraction (XRD) patters of the pyrolytic products from $ZnCl_2$●Chitosan precursors (1:1. 1:5, and 1:10) showed the main peaks corresponding to hexagonal phase of the ZnO. For instance, the pyrolysis of 1:1 $ZnCl_2$●Chitosan precursors led to a diffractogram pattern with peaks at 2θ values of 31.88°, 34.53°, 36.36° and 56.70°, corresponding to the (100), (002) , (101) and (110) planes of the hexagonal phase of the ZnO (see Figure S5 in the Supplementary Materials). The analysis of these hexagonal ZnO phases by SEM clearly showed a dependence of the morphology with the [polymer/metal] molar ratio of the precursors (Figure 1). Thus, when $ZnCl_2$●Chitosan having [polymer/metal] molar ratios of 1:1 and 1:5 were used as precursors, SEM images showed very compacted and homogeneous ZnO morphologies (see Figure 1a and 1b respectively), whereas when the 1:10 [polymer/metal] molar ratio precursor was used, porous ZnO materials were obtained (see Figure 1c). The higher dispersion of the metal moiety in the 1:10 $ZnCl_2$●Chitosan precursor with respect to that of the 1:1 and 1:5, may explain the less homogeneous texture of the 1:10 precursor, leading to porous ZnO materials.

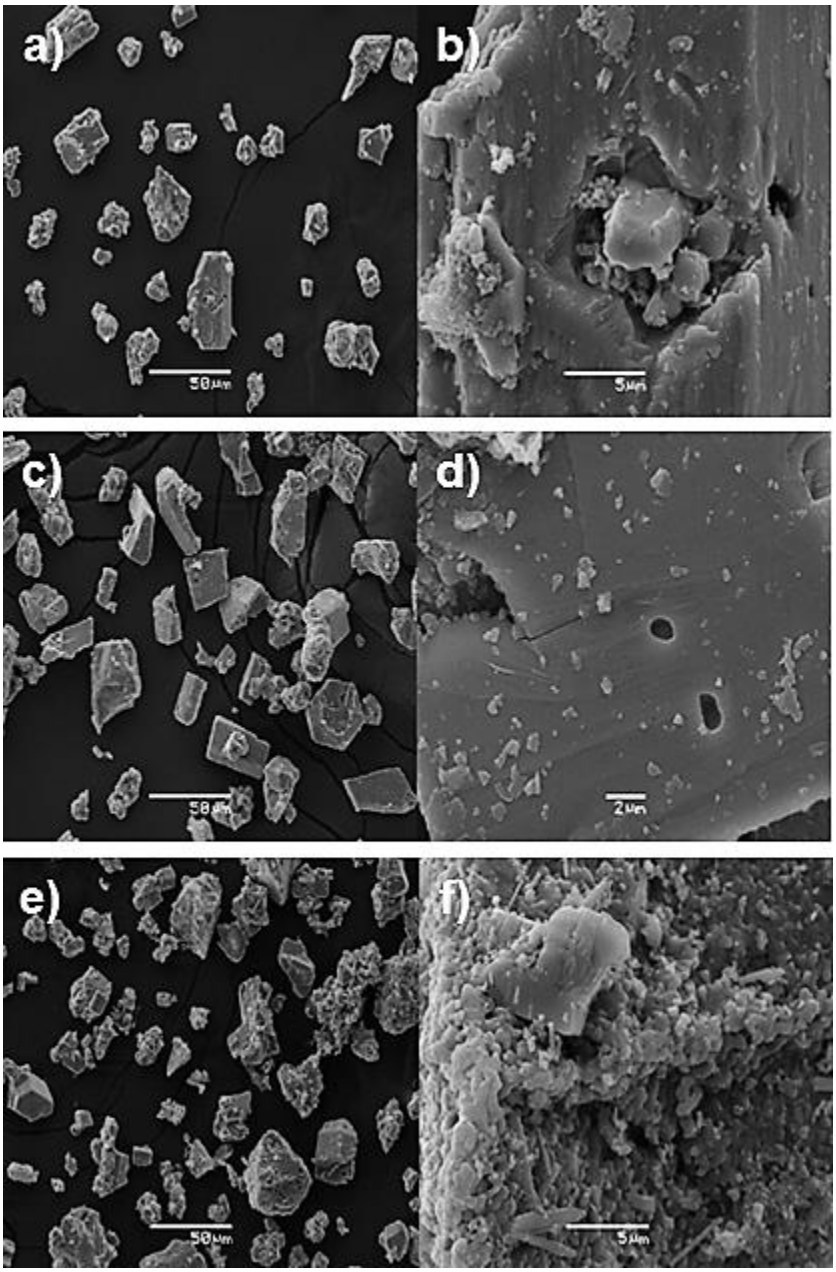

Figure 1 SEM images at different magnifications of ZnO nanomaterials synthesized from $ZnCl_2$●Chitosan precursors having different [polymer/metal] molar ratios: (a,b) 1:1, (c,d) 1:5 and (e,f) 1:10.

The EDX analysis of the materials prepared from the different $ZnCl_2$●Chitosan precursors ([polymer/metal] molar ratios of 1:1, 1:5, and 1:10), confirmed the presence of ZnO materials by the presence of Zn and O elements (see Figure S6 in the Supplementary Materials).

The as obtained ZnO materials were also analyzed by TEM. As it is usually found from a variety of preparation methods involving thermal treatments, a wide particle size distribution was observed (see Figure 2). However, a closely look to the micrographs showed a slightly different size distribution of the nanostructures of ZnO depending of the different [polymer/metal] molar ratios used in the $ZnCl_2$●Chitosan precursors (see Figure 2). Thus, the smallest size ZnO nanoaggregates were observed when a 1:5 [polymer/metal] molar ratio of the $ZnCl_2$●Chitosan precursor was used (see Figure 2c). Interestingly, at this [polymer/metal] molar ratio of the $ZnCl_2$●Chitosan precursor (1:5), we observed the highest crystallinity in the electron diffraction pattern of the ZnO nanoparticles. So, at 1:5 [polymer/metal] molar ratio the crystallization of the hexagonal phase of the ZnO nanoparticles is favored with respect to the 1:1 and 1:10 [polymer/metal] molar ratios.

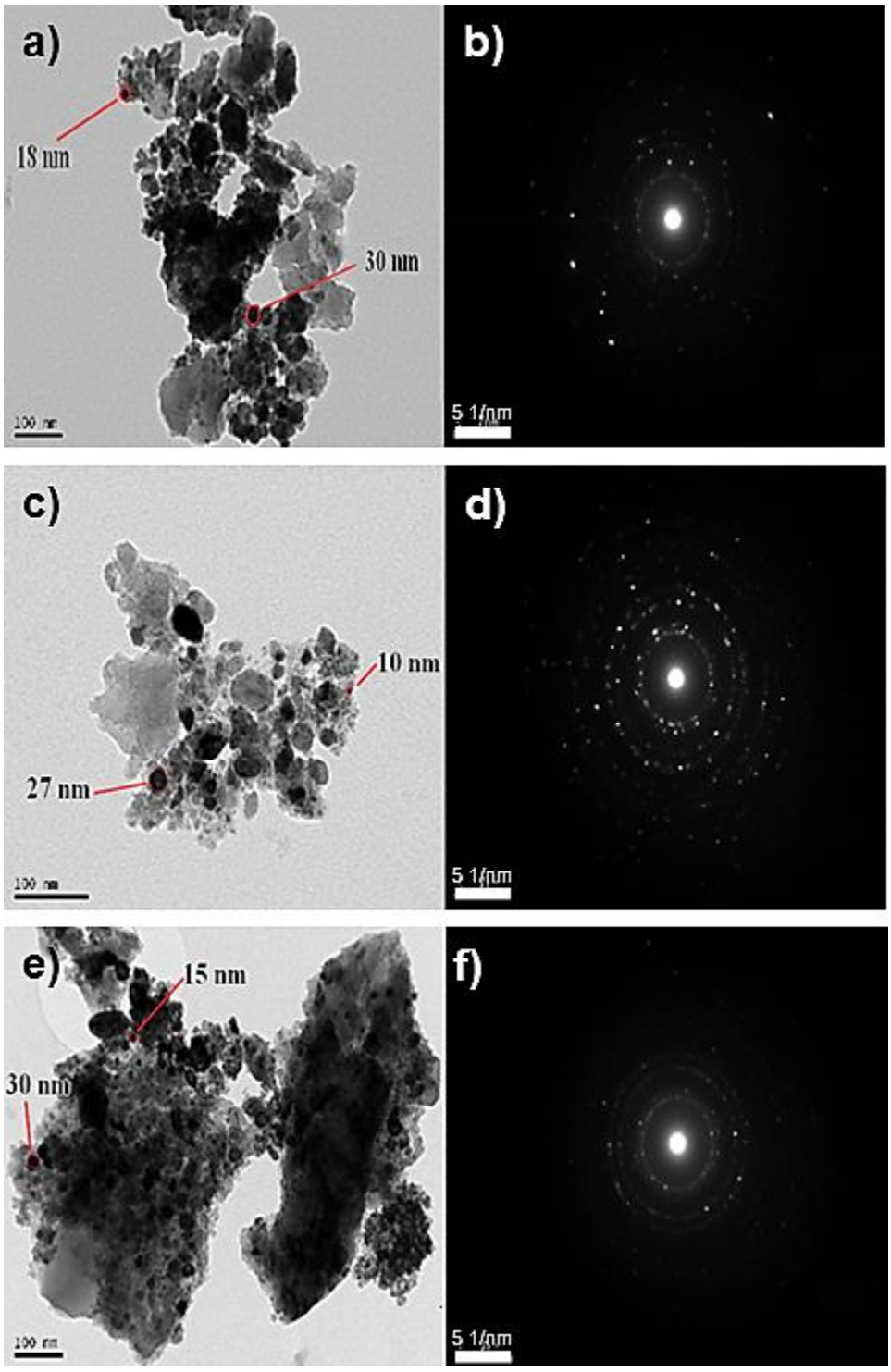

Figure 2 TEM images (left) and electron diffraction patterns (right) of the ZnO prepared from $ZnCl_2$●Chitosan in [polymer/metal] molar ratios of 1:1 (a,b), 1:5 (c,d), and 1:10 (e,f).

HR-TEM analysis was performed using a single crystal ZnO nanoparticles obtained from the 1:1 $ZnCl_2$●Chitosan precursor (see Figure 3).

The single ZnO nanoparticle exhibited fairly accurate hexagonal morphology with the particle size ranging from 6 to 40 nm. The measured lattice spacing of adjacent lattice planes was about 0.30 nm, corresponding to the (100) plane of hexagonal ZnO nanoparticles and grew along the [100] direction.

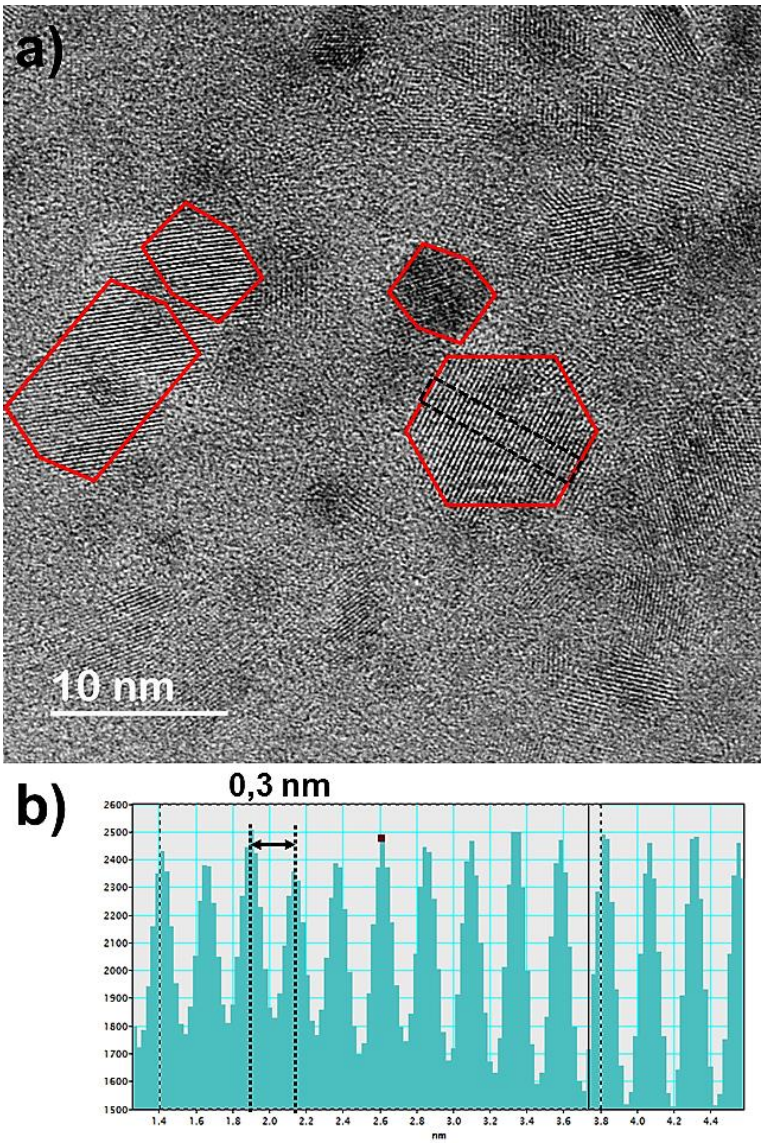

Figure 3. (a) HR-TEM of ZnO prepared from the 1:1 $ZnCl_2$●Chitosan precursor. (b) Measured lattice spacing of adjacent lattice planes of ZnO materials (dashed black squared area in Figure 3a).

2.2. Uv-vis and photoluminescence properties of ZnO materials. ZnO is an n-type semiconductor with a wide band gap of 3.37 eV in bulk. We studied the diffuse reflectance spectra (DRS) of the ZnO materials prepared from the 1:1. 1:5, and 1:10 $ZnCl_2$●Chitosan precursors at room temperature (see Figures 4a, 4c, and 4e. The reflectance data was converted to Kubelka-Munk equation using standard procedures). ZnO samples showed a strong absorption band in the region between 200 and 400 nm. Thus, the absorptions of ZnO are mainly located at the UV region, not observing intense absorptions in the visible region. This result is attributed to the direct band gap of ZnO due to electron transitions from the valence to the conduction band (O_{2p}–Zn_{3d}).[35] The optical band gap energies of the ZnO materials were estimated from Tauc's plot, $(\alpha h\nu)^2 = A(h\nu - E_g)$ (see Figures 4b, 4d and 4f). The band gap values of the E_g were found to be 2.25 (1:1 $ZnCl_2$●Chitosan precursor), 2.16 (1:5 $ZnCl_2$●Chitosan precursor) and 2,26 eV (1:10 $ZnCl_2$●Chitosan precursor). The values are slightly different depending on the [polymer/metal] molar ratio of the $ZnCl_2$●Chitosan precursors. Furthermore, the values are lower than that reported for bulk samples of ZnO (3.37 eV), and also lower with respect to ZnO materials prepared by related methods,[36,37] which can be explained by the high crystallinity and large particle size aggregates observed in the electron diffraction patters and TEM micrograph respectively (see Figure 2).[38,39] Additionally, the presence of residual carbon impurities[36] and the high temperatures used during the ZnO formation,[37] can be also accounted for the low values of the E_g obtained.

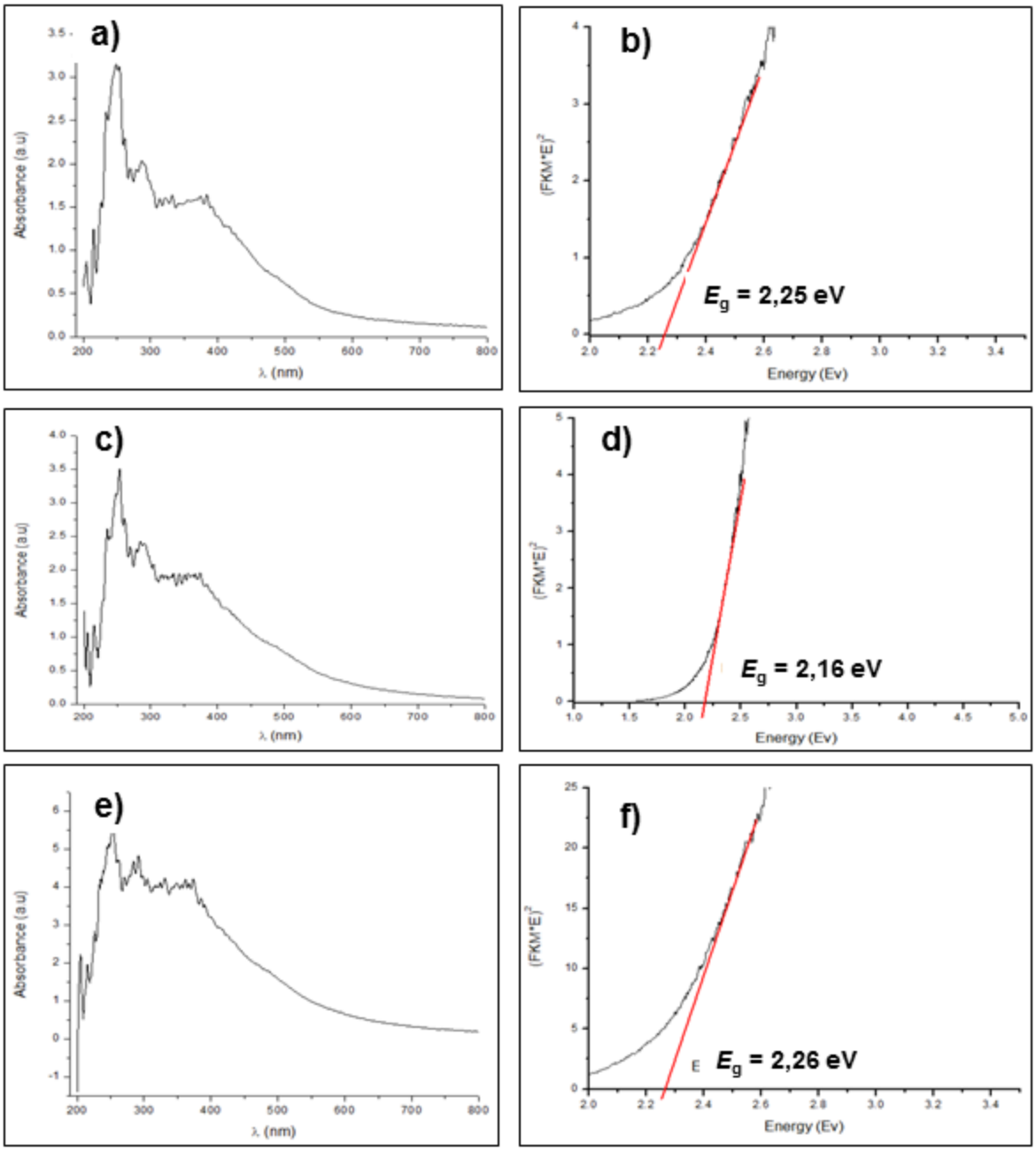

Figure 4 Uv-vis absorption and reflectance data (converted to Kubelka Munk spectra) of ZnO nanoparticles created by the $ZnCl_2$●Chitosan precursors at different [polymer/metal] molar ratios: (a) 1:1, (c) 1:5, and (e) 1:10. Tauc's plot, $(\alpha h\nu)^2 = A(h\nu - E_g)$ having the optical band energy (E_g) of ZnO nanoparticles created by the $ZnCl_2$●Chitosan precursors at different [polymer/metal] molar ratios: (b) 1:1, (d) 1:5, and (f) 1:10.

The photoluminescence spectra of the as prepared ZnO materials (Figure 5), showed four different emission peaks at 354 nm, 392-395 nm, 423 nm, and 566-573 nm. By comparison with the emission spectra pattern of ZnO materials

obtained by related methods, these emission peaks are assigned as follows: The strong Uv-vis bands at 354 and 392 nm correspond to the exciton recombination related to the near-band edge (NBE) emissions of ZnO; the blue emission (423 nm) corresponds to the electron transition to the conductive band to interstitials oxygen defects (O_{in}) in the ZnO; and finally, the observed emission band at 560 nm (green emission) could be assigned to a several effects such as the transition between singly charged oxygen vacancy and photoexcited hole,[40,41] the transition between the electron close to the conduction band and deeply trapped hole at V_o^{++} center (oxygen vacancy containing no electrons),[42-44] the donor–acceptor and shallow donor–deep level transitions,[45-47] the zinc interstitials,[48] and the oxygen antisites.[49] Similar photoluminescence peaks have been obtained for ZnO B-doped materials.[50]

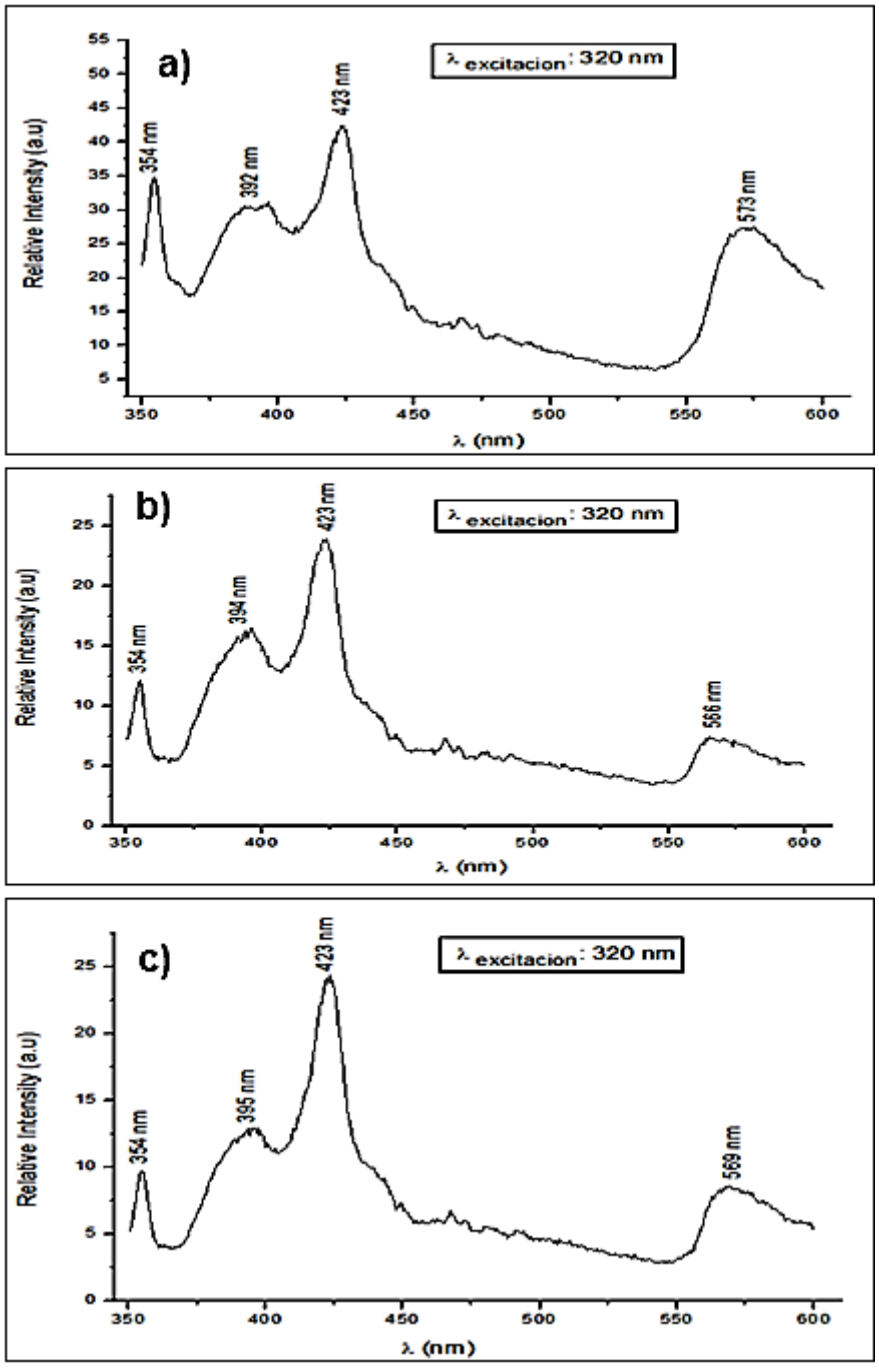

Figure 5 Luminescence spectra of ZnO nanoparticles created by the $ZnCl_2$●Chitosan precursors at different [polymer/metal] molar ratios: (a) 1:1, (b) 1:5, and (c) 1:10.

3. Characterization of the SnO_2 materials

3.1. Crystallographic and electronic microscopy characterization of SnO_2 materials.

The XRD pattern analysis for the pyrolytic products from precursor $SnCl_2$●Chitosan in [polymer/metal] molar ratios of 1:1, 1:5, and 1:10, showed the presence of pure SnO_2 cassiterite-synphase. The main observed reflections at $2\theta = 26.08°$, 33.89°, 37.96°, 51.80°and 54.67° can be indexed to the spacing (110), (101), (200) , (211) and (220) respectively (see Figure S6 in the Supplementary Materials).

The analysis of the as prepared SnO_2 cassiterite-synphases by SEM, clearly showed dependence of the morphology with the [polymer/metal] molar ratio of the precursors $SnCl_2$●Chitosan (Figure 6). Thus, when $SnCl_2$●Chitosan having [polymer/metal] molar ratio of 1:1 was used as precursor, the SEM images showed a non-compacted porous materials having a foam-like texture (see Figure 6a), whereas when the 1:5 and 1:10 [polymer/metal] molar ratios of the $SnCl_2$●Chitosan precursor was used, mixtures of foam-like textures and rod-like nanostructures were clearly observed (see Figure 6b-c in which nanorods are highlighted with white arrows).

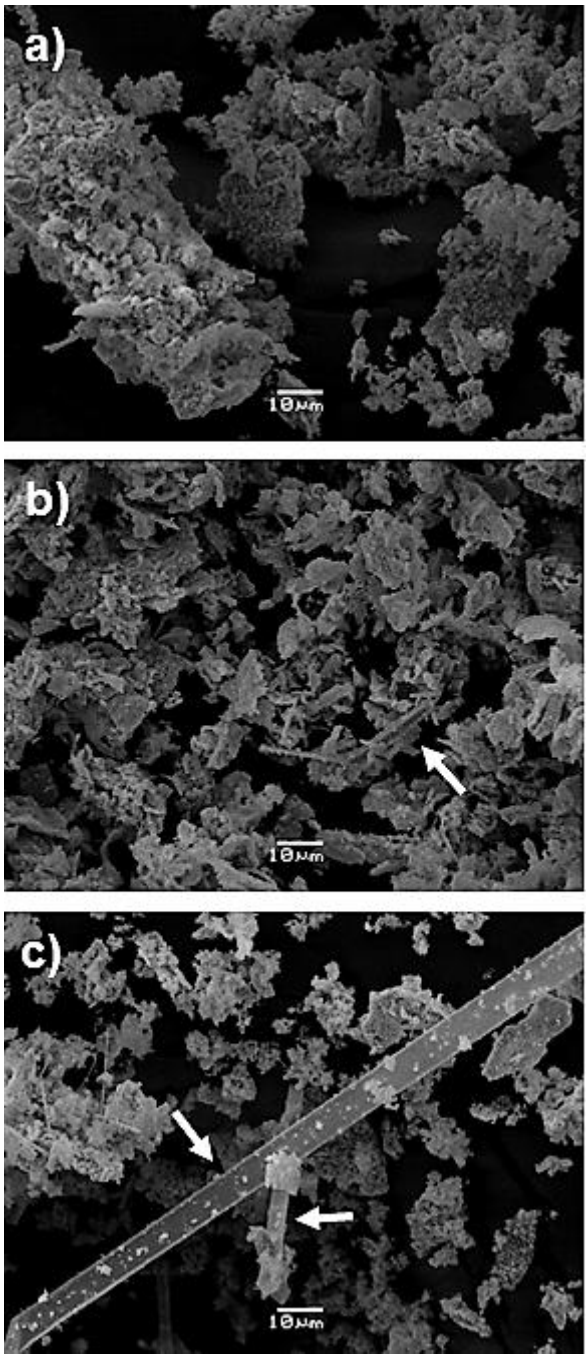

Figure 6 SEM images showing the morphology of the SnO_2 materials prepared from precursor $SnCl_2$●Chitosan in [polymer/metal] molar ratios of 1:1 (a), 1:5 (b), and 1:10 (c). White arrows highlight the nanorod-like morphologies.

SnO_2 materials were analyzed by TEM observing a slightly different size distribution of the nanostructures depending of the different [polymer/metal] molar ratios used in the $SnCl_2$●Chitosan precursors (see Figure 7). Thus, the smallest size SnO_2 nanoaggregates were observed when a 1:5 [polymer/metal] molar ratio of the $SnCl_2$●Chitosan precursor was used (see Figure 7c). Interestingly, at this [polymer/metal] molar ratio of the $SnCl_2$●Chitosan precursor (1:5), we observed areas in which very small and almost uniform SnO_2 nanoparticles were formed (particle diameter average of 2.1 ± 0.2 nm). Moreover, these small size nanoparticles exhibited a directional dispersity probably due to the dewetting of the solvent during the casting of the sample over the carbon coated copper grid (see Figure 7d). The electron diffraction pattern of the SnO_2 material obtained from the different $SnCl_2$●Chitosan precursors evidenced the crystalline nature of the pyrolytic SnO_2 products obtained by this methodology (see Figure 7f).

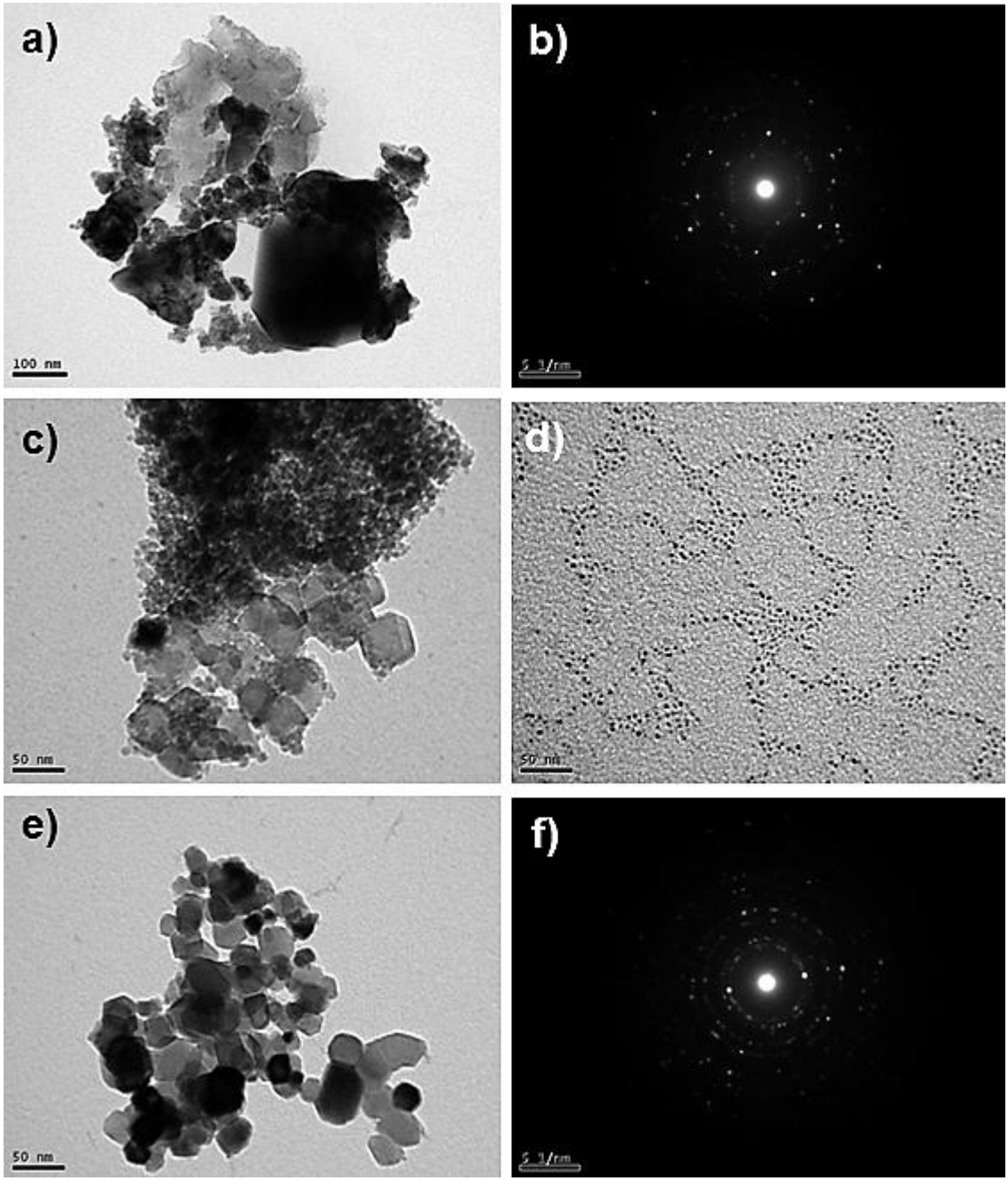

Figure 7 TEM images and electron diffraction patterns of the SnO_2 obtained from $SnCl_2$●Chitosan having [polymer/metal] molar ratio of 1:1 (a,b); 1:5 (c,d); and 1:10 (e,f).

HRTEM analysis was performed using a single crystal SnO_2 nanoparticle obtained from the 1:1 $SnCl_2$●Chitosan precursor (see Figure 8a). The measured lattice spacing of adjacent lattice planes was about 0.26 nm, which corresponds to the (101) plane of tetragonal SnO_2 nanoparticles cassiterite-synphase, and grew along the [101] direction. The polycrystal-line diffraction rings of electron

diffraction pattern patterns (see Figures 8b and 8d) also demonstrate the microstructural character of the typical tetragonal cassiterite SnO_2 phase (d_{101} = 0.26 nm and d_{110} = 0.34 nm)

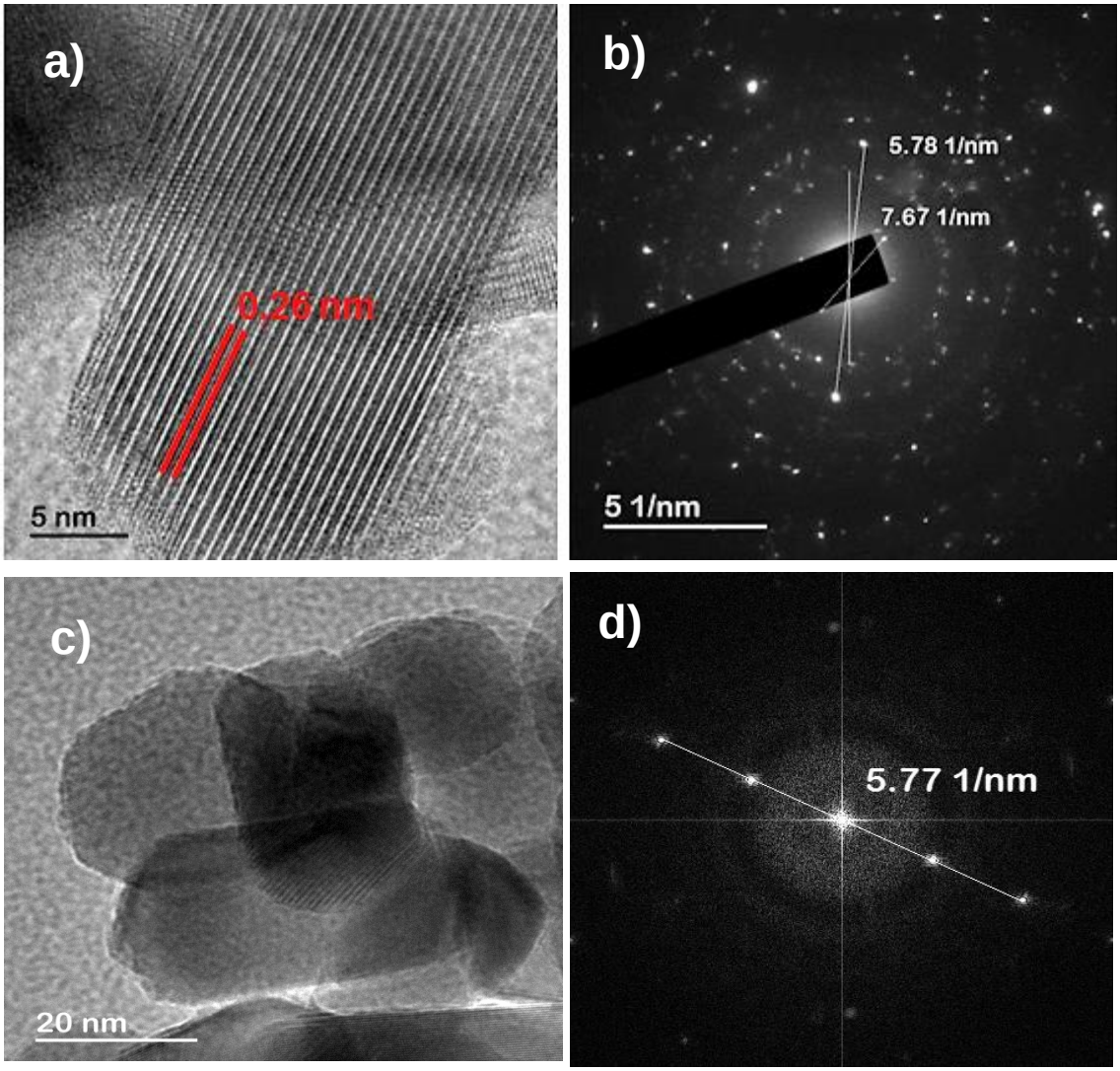

Figure 8. HR-TEM (a,c) and electron diffraction patterns (b,d) images of SnO_2 prepared from the 1:1 precursor $SnCl_2$●Chitosan.

3.2 Uv-absorption and photoluminescence study of the SnO_2 materials.

We studied the diffuse reflectance spectra (DRS) of the SnO_2 materials prepared from the 1:1. 1:5 and 1:10 $SnCl_2$●Chitosan precursors at room temperature (see Figures 9a, 9c, and 9e. The reflectance data was converted to Kubelka-Munk equation using standard procedures). SnO_2 materials showed a strong and broad absorption band in the region from 200 to 400 nm, being located the maximum of the absorption band at *ca*. 250 nm. The optical band gap energies of the products were estimated from Tauc's plot, (see Figures 9b, 9d and 9f). The band gap values of the E_g were found to be 4.42 (1:1 $SnCl_2$●Chitosan precursor), 4.40 (1:5 $SnCl_2$●Chitosan precursor), and 4.48 eV (1:10 $SnCl_2$●Chitosan precursor). The values are slightly different depending on the [polymer/metal] molar ratio of the $SnCl_2$●Chitosan precursors. The values are higher than those reported for bulk samples of SnO_2 (3.64 eV), and also higher than those of the SnO_2 materials prepared by related methods.[51,52] These higher values of the E_g of the as synthesized SnO_2 materials can be related with the large particle size aggregates observed in the TEM micrographs (see Figure 7), and the high temperature used during the pyrolysis process.[51]

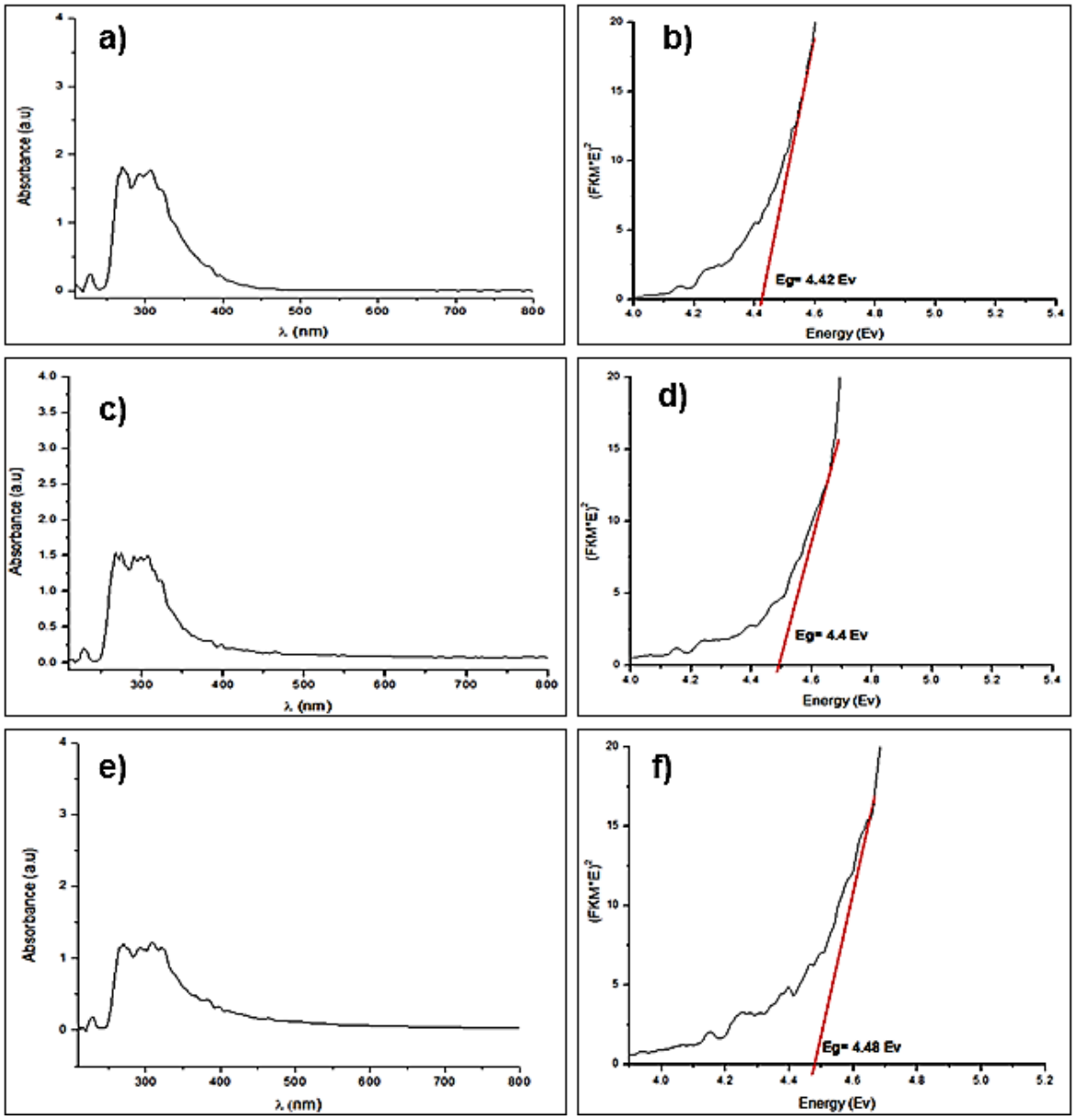

Figure 9 UV-vis absorption and reflectance data (converted to KubelkaMunk spectra) of SnO_2 nanoparticles created by the $SnCl_2$●Chitosan precursors at different [polymer/metal] molar ratios: (a) 1:1, (c) 1:5, and (e) 1:10. Tauc's plot, $(\alpha hv)^2 = A(hv\text{-}E_g)$ having the optical band energy (E_g) of SnO_2 nanoparticles created by the $SnCl_2$●Chitosanpprecursors at different [polymer/metal] molar ratios: (b) 1:1, (d) 1:5, and (f) 1:10.

The photoluminescence spectra of the as prepared SnO_2 exhibited an intense blue luminescence at a wavelength of 420 nm (see Figure 9) which may be attributed to oxygen-related defects that have been introduced during the growth process.[52-54] Furthermore an additional weak emission at 680 nm was

observed (see Figure 9), which can be attributed to small traces of impurities during sample preparation.[53]

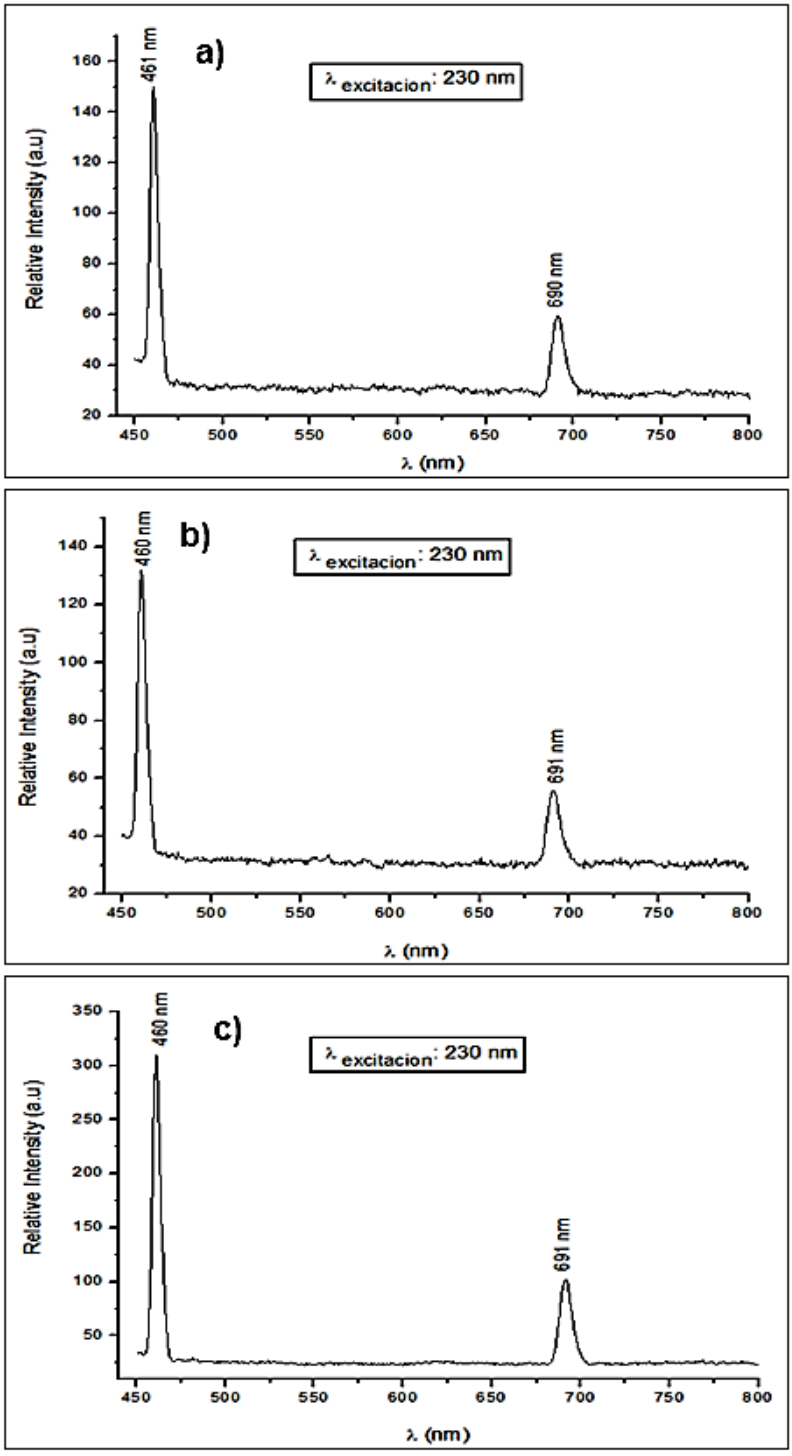

Figure 10 Luminescence spectra of SnO_2 nanoparticles created by pyrolysis of the $SnCl_2$●Chitosan precursors having different [polymer/metal] molar ratios: (a) 1:1, (b) 1:5, and (c) 1:10.

4. Incorporation of ZnO and SnO_2 into SiO_2

Incorporation of ZnO and SnO_2 into SiO_2 was achieved by pyrolysis of mixtures of MCl_2●Chitosan (M= Zn and Sn) precursors and SiO_2 (SiO_2 was synthesized by a sol-gel method). The XRD diffraction patterns of the isolated products (see Figure S7) obtained after the pyrolysis, showed the peaks corresponding to the incorporation of SnO_2 into the SiO_2 (SnO_2 //SiO_2). However, the pyrolysis of the mixtures $ZnCl_2$●Chitosan and SiO_2 led to Zn_2SiO_4 and SiO_2 (see XRD in Figure S7). The SnO_2//SiO_2 material was further analyzed by SEM and EDS mapping analyses (Figure 11). The images clearly showed the presence of SnO_2 homogeneously distributed into the SiO_2 matrix (see Figure 11). The UV-visible diffuse reflectance spectra of the SnO_2 //SiO_2 materials was very similar to that of pure SnO_2 (i.e. without SiO_2),[52-54] and similar to that different SnO_2 //SiO_2 materials prepared by related synthetic methodologies.[55] The band gap value estimated using the Tauc approximation for SnO_2//SiO_2 materials was 3.1 eV, significantly lower than that obtained for pure SnO_2 prepared by pyrolysis (ca. 4.4 eV, see discussion above). This lower value might be due to the presence of the amorphous silica that precludes the formation of large SnO_2 nanoparticles (see the Sn mapping in Figure 11), leading, therefore, to E_g value very similar to that of the pure SnO_2 (ca. 3.0 ev).[51]

The photoluminescence spectrum of SnO_2//SiO_2 (see Figure S8 in the Supplementary Materials) exhibited a strong near-Uv luminescence emission (ca. 400 nm), which is very similar to that observed in SnO_2//SiO_2 obtained by solution methods.[55] However, some important differences can be observed with respect to the luminescence spectrum of pure SnO_2 obtained by direct pyrolysis of the $SnCl_2$●Chitosan precursors. The emission peak observed at 690 nm for the last was not observed in the spectrum of the SnO_2 included in SiO_2.

Also the emission peak at 420 nm observed for pure SnO_2 was shifted to 400nm. These changes are due to the different oxygen-related defects that have been introduced during the inclusion process.

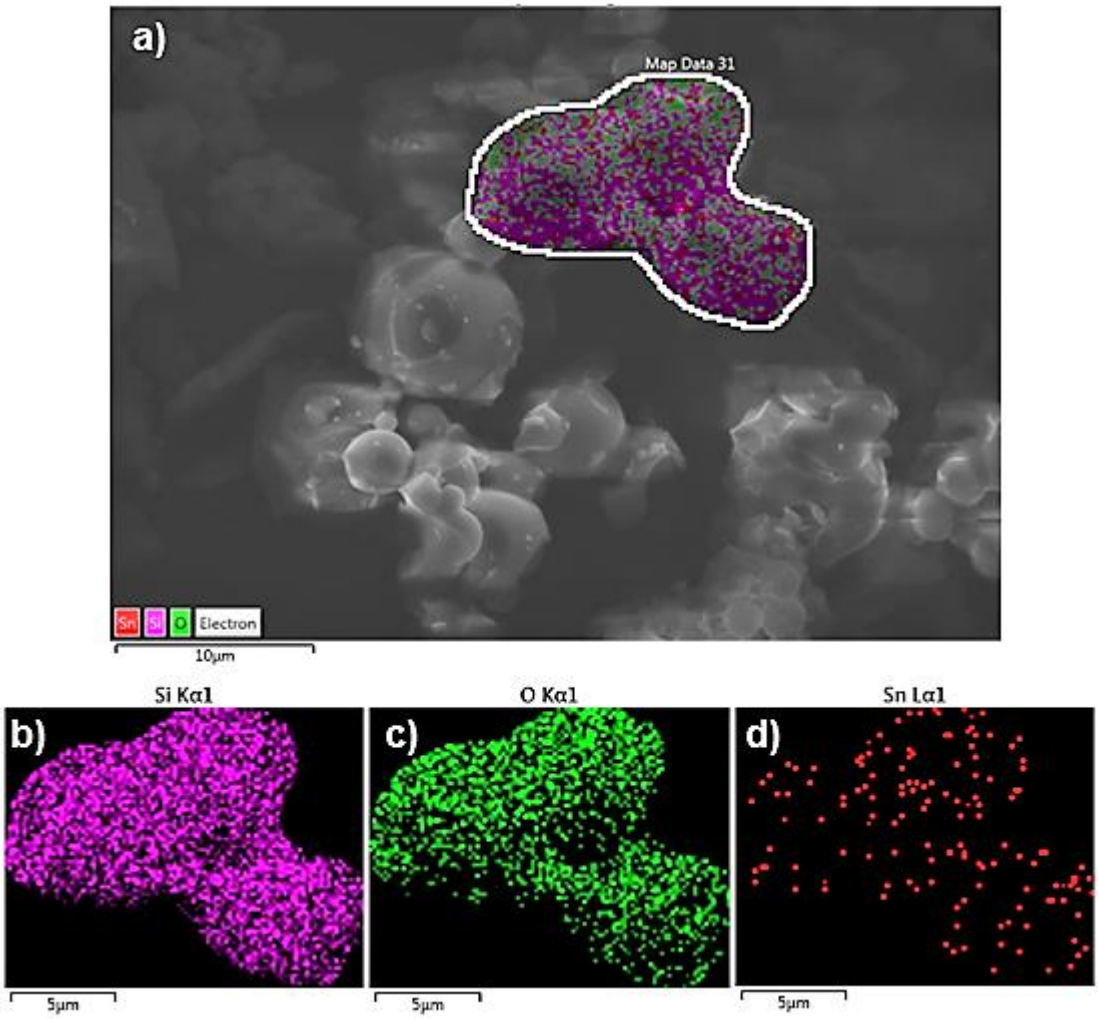

Figure 11 SEM analysis of SnO_2//SiO_2 materials showing an EDS mapping analyses of elements in a grain of material. Elements: Sn (red), Si (purple), and oxygen (green).

Conclusions

In conclusion, nanoparticles of ZnO and SnO_2 have been conveniently prepared by a solid-state method based on the pyrolysis (800 ºC, air) of hybrid macromolecular precursors $ZnCl_2$●Chitosan and $SnCl_2$●Chitosan having different [polymer/MCl_2] (M = Zn or Sn) ratios (1:1, 1:5 and 1:10). The

morphology and size of the nanostructured ZnO and SnO_2 materials can be controlled by varying the [polymer/MCl_2] ratio in the MCl_2●Chitosan (M = Zn, Sn) precursors. Thus, the smallest size oxides were obtained by using the 1:5 polymer/metal ratio. As prepared ZnO materials exhibit luminescence spectra having the most intense emission at 440 nm, which corresponds to a radiative transition of an electron from the shallow donor level of oxygen vacancies, and the zinc interstitial, to the valence band. Furthermore, ZnO materials show a rather intense green emission at ca. 573 nm, which is characteristic of this synthetic methodology. On the other hand, the photoluminescence spectrum of the nanostructured SnO_2 shows an intense blue luminescence at a wavelength of 420 nm which may be attributed to oxygen-related defects that have been introduced during the growth process of the nanoparticles. The absorption and luminescence properties of as prepared ZnO and SnO_2 materials showed a very small dependence of the [polymer/metal] molar ratio of the MCl_2●Chitosan (M = Zn, Sn) precursors used in their preparation. In other hand, whereas SnO_2 was successfully incorporated into SiO_2 structure (SnO_2//SiO_2) by pyrolysis of solid-state mixtures of the precursors $SnCl_2$●Chitosan in the presence of SiO_2, the same reaction carried out with $ZnCl_2$●Chitosan precursors led to a mixture of Zn_2SiO_4 and SiO_2 The absorption and photoluminescence properties of the nanostructured SnO_2//SiO_2 were very similar than those of pure SnO_2.

Acknowledgements: C.D. is grateful to Fondecyt (Project 1160241) for the funding. A.P.S. is grateful to FICYT (Projects SV-PA-13-ECOEMP-83 and FC-15-GRUPIN14-106), Universidad de Oviedo (Project UNOV-13-EMERG-GIJON-08) and the MINECO (Project CTQ2014-56345-P) for the funding. A.P.S. is also grateful to the COST action Smart Inorganic Polymers (SIPs-

CM1302 - http://www.sips-cost.org/home/index.html), and the Juan de la Cierva and Ramón y Cajal programs.

Notes: The authors declare no competing financial interest.

Supplementary Materials. Experimental details, ^{13}C CP-MAS NMR spectroscopy, XRD patterns, EDX analysis, and TGA/DTA curves of the MCl_2·Chitosan (M = Zn and Sn) precursors, and metal oxide (ZnO and SnO2) materials, are included

References

[1] Joshi RK, Schneider JJ (2012) Assembly of one dimensional inorganic nanostructures into functional 2D and 3D architectures. Synthesis, arrangement and functionality. Chem Soc Rev 41: 5285-5312.

[2] Poizot P, Grugeon LS, Dupont L, Tarascon JM (2000) Nano-sized transition-metal oxides as negative-electrode materials for lithium-ion batteries. Nature 407: 496-499.

[3] Li Y, Somorjai GA (2010) Nanoscale Advances in Catalysis and Energy Applications. Nano Lett 10: 2289-2295.

[4] Zhang Q, Wang HY, Xinli J,Yang Y (2013) One-dimensional metal oxide nanostructures for heterogeneous catalysis. Nanoscale 5: 7175-7183.

[5] Wang H, Rogach AL (2014) Hierarchical SnO_2 Nanostructures: Recent Advances in Design, Synthesis, and Applications. Chem Mater 26: 123–133.

[6] Ahmad M, Zhu JJ (2011) ZnO based advanced functional nanostructures: synthesis, properties and applications. J Mater Chem 21: 599-614.

[7] Tricoli A, Righettoni M, Teleki A (2010) Semiconductor Gas Sensors: Dry Synthesis and Application. Angew Chem Int Ed. 49:7632-7659.

[8] Juttukonda V, Paddock RL, Raymond JE, Denomme D, Richardson AE, Slusher L, Fahlman BD (2006) Facile Synthesis of Tin Oxide Nanoparticles Stabilized by Dendritic Polymers. J Am Chem Soc 128: 420-421.

[9] Sun JQ, Wang JS, Wu XC, Zhang GS, Wei JY, Zhang SQ, Li H, Chen DR (2006) Novel Method for High-Yield Synthesis of Rutile SnO2 Nanorods by Oriented Aggregation. Crystal Growth and Design 6:1584-1587.

[10] Salvat-Niasari M, Mir N, Davar F (2010) Synthesis, characterization and optical properties of tin oxide nanoclusters prepared from a novel precursor via thermal decomposition route. Inorg Chim Acta 363: 1719-1726.

[11] Zereie M, Gholami A, Bahrami M, Rezaei AH (2013) A simple method for preparation of micro-sized ZnO flakes. Mat Lett 91: 255-257.

[12] Hossienifard M, Hashemi L, Amani V, Kalatech K, Morsali A (2011) Synthesis and Characterization of ZnO Nanoparticles via Thermal Decomposition of Two Zinc(II) Supramolecular Compounds. J Inorg Organomet Polym 21: 527-533.

[13] Díaz C, Valenzuela ML (2011) Metallic Nanostructures using Oligo and Polyphosphazenes as Template/stabilizer in solid state in Encyclopedia of Nanoscience and Nanotechnology Nalwa HS Ed. American Scientific16: 239-256.

[14] Díaz C, Valenzuela ML (2006) Organometallic Derivatives of Polyphosphazenes as Precursors for Metallic Nanostructured Materials. J Inorg and Organometallic Polym 16: 419-435.

[15] Díaz C, Valenzuela ML, Zuñiga L, O'Dwyer C (2009) Organometallic derivatives of cyclotriphosphazene as precursors of Nanostructured metallic materials: A new solid state Method. J Inorg and Organometallic Polym 19: 507-520.

[16] Díaz C, Valenzuela ML, Lavayen V, O'Dwyer C (2012) Layered Graphitic Carbon Host Formation during Liquid-free Solid State Growth of Metal Pyrophosphates. Inorg Chem 51: 6228-6236.

[17] Diaz C, Carriedo GA, Valenzuela ML, Zuñiga L, O'Dwyer C (2012) Polymer/Trimer/Metal Complex Mixtures as Precursors of Gold Nanoparticles: Tuning the Morphology in the Solid-State. J Inorg and Organometallic Polym Mater 22: 447-454.

[18] Díaz C, Valenzuela ML, Cáceres S, O´Dwyer C (2013) Solution and surfactant-free growth of supported high index facet SERS active nanoparticles of rhenium by phase demixing. J Mat Chem A 1: 1566-1572.

[19] Wan-Ngah WS, Teong LC, Hanafiah MAKM (2011) Adsorption of dyes and heavy metal ions by chitosan composites: A review. Carbohydrate Polymers 83: 1446-1456.

[20] Aranaz I, Mengibar M, Harris R, Paños I, Miralles B, Acosta N, Galed G, Heras A (2009) A functional characterization of chitin and chitosan regarding some biological properties and some specific applications. Current Chemical Biology 3: 203-230.

[21] Okuyama K, Noguchi K, Miyazawa T, Yui T, Ogawa K (1997) Molecular and Crystal Structure of Hydrated Chitosan. Macromolecules 30: 5849-5855.

[22] Mazeau K, Winter WT, Chanzy JH (1994) Molecular and crystal structure of a high-temperature polymorph of chitosan from electron diffraction data. Macromolecules 27: 7606-7612.

[23] Muzzarelli A (1973) "Chitin" Pergamon Press, New York.

[24] Majeti RMNV, Kumar R (2000) A review of chitin and chitosan applications. Reactive Functional Polymers 46: 1-27.

[25] Kong M, Chen XG, Xing K, Park HJ (2010) Antimicrobial properties of chitosan and mode of action: A state of the art review. International Journal of Food Microbiology 144: 51-63.

[26] Crini G, Badot PM (2008) Application of chitosan, a natural aminopolysaccharide, for dye removal from aqueous solutions by adsorption processes using batch studies: A review of recent literature. Prog Polym Sci 33: 399-447.

[27] Chin F, Tseng RL, Juang RS (2010) A review and experimental verification of using chitosan and its derivatives as adsorbents for selected heavy metals. Journal of Environmental Management 91: 798-806.

[28] Emara AAA, Tawad MA, El-ghamry MA, Elsabee MZ (2011) Metal uptake by chitosan derivatives and structure studies of the polymer metal complexes. Carbohydrate Polymers. 83, 192-202.

[29] Ozawa K, Oka K, Yui T (1993) X-ray study of chitosan-transition metal complexes. Chem Mater 5: 726-728.

[30] Schlick Sh (1986) Binding sites of copper$_{2+}$ in chitin and chitosan. An electron spin resonance study. Macromolecules 19: 192-195.

[31] Rinaudo M (2006) Chitin and chitosan: Properties and applications. Prog Polym Sci 31: 603-632.

[32] Sine A, Petersen BO, Duus JO, Skrydstrup T (2007) Studies Directed to Understanding the Structure of Chitosan−Metal Complexes: Investigations of Mono- and Disaccharide Models with Platinum(II) Group Metals. Inorg Chem 46: 4326-4335

[33] Heux L, Brugnerotto J, Desbrieres J, Versali MF, Rinaudo M (2000) Solid State NMR for Determination of Degree of Acetylation of Chitin and Chitosan. Biomacromolecules 1: 746-751.

[34] De Brito D, Campana-Filho SP (2007) Kinetics of the thermal degradation of chitosan. Thermochimica Acta 465: 73-82.

[35] Anandam M, Dinesh S, Krishnakumar N J Mater Sci Mater Electron DOI 10.1007/s10854-016-5833-2

[36] Samadi M, Asghari H, Pourjavadi A, Moshfegh AZ (2013) Synergism of oxygen vacancy and carbonaceous species on enhanced photocatalytic activity of electrospun ZnO-carbon nanofibers: Charge carrier scavengers mechanism. Appl Cat A 466: 153-160.
[37] Vinodkumar R, Navas I, Porsezian K, Ganesan V, Unnikrishnan NV, Pillai VPM (2014) Structural, spectroscopic and electrical studies of nanostructured porous ZnO thin films prepared by pulsed laser deposition. Spectrochim Acta A118: 724-732.
[38] Sowri Babu K, Ramachandra Reddy A, Sujatha Ch, Venugopal Reddy K, Mallika AN (2013) Synthesis and optical characterization of porous ZnO. J Adv Ceram 2: 260-265.

[39] Mathewa JP, Vargheseb G, Mathewa J (2012) Effect of post-thermal annealing on the structural and optical properties of ZnO thin films prepared from a polymer precursor. Chin Phys B 21: 078104.

[40] Vanheusden K, Seager CH, Warren WL, Tallant DR, Voigt JA (1998) Correlation between photoluminescence and oxygen vacancies in ZnO phosphors. Appl Phys Lett 68: 403-405.
[41] Vanheusden K, Warren WL, Seager CH, Tallant DR, Voigt JA, Gnade BE (1996) Mechanisms behind green photoluminescence in ZnO phosphor powders. J Appl Phys 79: 7983-7990.
[42] Van Dijken A, Meulenkamp E, Vanmaekelbergh D, Meijerink A (2000) The Kinetics of the Radiative and Nonradiative Processes in Nanocrystalline ZnO Particles upon Photoexcitation. J Phys Chem B 104: 1715-1723.
[43] Van Dijken A, Meulenkamp E, Vanmaekelbergh D, Meijerink A (2000) Identification of the transition responsible for the visible emission in ZnO using quantum size effects. Journal of Luminescence 90: 123-128.

[44] Wood A, Giersig M, Hilgendorff M, Vilas-Campos A, Liz-Marzán LM, Mulvaney P (2003) Size Effects in ZnO: The Cluster to Quantum Dot Transition. Australian J Chem 56: 1051-1057.

[45] Reynolds DC, Look DC, Jogai B, Morkoç H (1997) Similarities in the bandedge and deep-centre photoluminescence mechanisms of ZnO and GaN. Solid State Commun 101: 643-646.

[46] Studenikin SA, Cocivera M (2002) Time-resolved luminescence and photoconductivity of polycrystalline ZnO films. J Appl Phys 91: 5060-5065.

[47] Reynolds DC, Look DC, Jogai B (2001) Fine structure on the green band in ZnO. J Appl Phys 89: 6189-6191.

[48] Liu M, Kitai AH, Mascher P (1992) Point defects and luminescence centres in zinc oxide and zinc oxide doped with manganese. Journal of Luminescence 54: 35-42.

[49] Lin B, Fu Z, Jia Y (2001) Green luminescent center in undoped zinc oxide films deposited on silicon substrates**.** Appl Phys Lett 79: 943-945.

[50] Gomathisankar P, Hachisuka K, Katsumata H, Suzuki T, Funasaka K, Kaneco S (2013) Photocatalytic Hydrogen Production from Aqueous Na2S + Na2SO3 Solution with B-Doped ZnO. A C Sustainable Chem Eng 1: 982-988.

[51] Chetri P, Choudhury A (2013) Investigation of optical properties of SnO2 nanoparticles. Physica E 47: 257-263.

[52] Rajendran V, Anandan K (2012) Size, morphology and optical properties of SnO_2 nanoparticles synthesized by facile surfactant-assisted solvothermal processing. Material Science in Semiconductor Processing 15: 393-400.

[53] Her YCh, Hu JY (2006) Low-temperature growth and blue luminescence of SnO2 nanoblades. Appl Phys Let. 89: 043115.

[54] Liu B, Cheng CW, Chen R, Shen ZX, Fan HJ, Sun HD (2010) Fine Structure of Ultraviolet Photoluminescence of Tin Oxide Nanowires. J Phys Chem 114: 3407-3410.

[55] Liu ZC, Chen HR, Huang WM, Gu JL, Bu WB, Hua ZL, Shi JL (2006) Synthesis of a new SnO_2/mesoporous silica composite with room temperature photoluminescence. Micropor Mesopor Mater 89: 270-275.

For Table of Content

Nanostructured ZnO and SnO_2 materials are prepared by a solid-state method based on the pyrolysis of hybrid macromolecular precursors $ZnCl_2$●Chitosan and $SnCl_2$●Chitosan having different [polymer/MCl_2] (M = Zn or Sn) ratios (1:1, 1:5 and 1:10).

C. Diaz[a*], M. L.Valenzuela[b], M. Segovia, K. Correa[a], R. de la Campa[c] and A. Presa Soto[c]

Solid-state synthesis and optical properties of ZnO and SnO_2 nanoparticles and their nanocomposites with SiO_2.

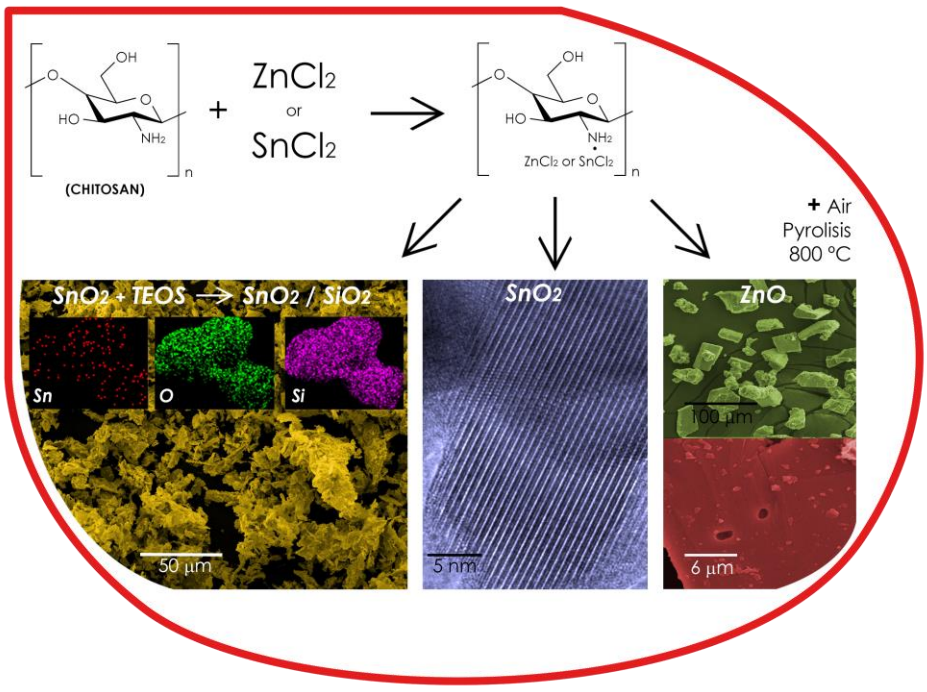
OH
HO
NH2
O
n
(CHITOSAN)
+
ZnCl2
or
SnCl2
ZnCl2 or SnCl2
+ Air
Pyrolisis
800 °C
SnO2 + TEOS → SnO2 / SiO2
Sn
O
Si
50 µm
SnO2
5 nm
ZnO
100 µm
6 µm